



# RSSI-Based Distributed Control to Align Directional Antenna Pairs for UAV Communication

Ahmet Taha Koru D, Jiajian Chang D, and Yan Wan D, Senior Member, IEEE

Abstract—In a scenario where two unmanned aerial vehicles (UAVs) are equipped with directional antennas for point-to-point communication, maintaining highperformance communication requires continuous adjustment of antenna orientations. This article presents a novel received signal strength indicator-based nonlinear static state feedback control law to achieve this under the unknown motions of the UAVs and the absence of global positioning system data. Our proposed method ensures convergence to the best orientation for almost all initial states of the closed-loop system when the UAVs are stationary. Furthermore, the closed-loop system achieves tracking of the best orientation with an error during motion. We experimentally demonstrate the effectiveness of the proposed method in solving the directional antenna pair alignment problem.

Index Terms—Decentralized control, directional antennas, nonlinear control systems, received signal strength indicator, uav networks.

# I. INTRODUCTION

## A. Literature Review

NMANNED aerial vehicles (UAVs) enable rapid and secure access to remote areas. Therefore, they offer an effective solution for applications ranging from environmental monitoring to emergency response [1]. The inherent remoteness of these operations necessitates a robust communication network between UAVs. This network is crucial for real-time information exchange, including piloting commands, UAV locations, and possibly video streams. While cellular networks present a promising solution, they do not generally cover the airspace and are expensive to build to support UAV operations. In addition, they may become inaccessible (e.g., in wilderness search and rescue missions) or destroyed (e.g., in monitoring areas impacted

Manuscript received 21 January 2024; revised 26 March 2024; accepted 19 May 2024. Date of publication 6 June 2024; date of current version 16 August 2024. Recommended by Technical Editor M. Tavakoli and Senior Editor Q. Zou. This work was supported by National Science Foundation under Grant CNS-2235160. (Corresponding author: Ahmet Taha Koru.)

The authors are with the Department of Electrical Engineering, The University of Texas at Arlington, Arlington, TX 76019 USA (e-mail: ahmet.koru@uta.edu; jxc5658@mavs.uta.edu; yan.wan@uta.edu).

Color versions of one or more figures in this article are available at https://doi.org/10.1109/TMECH.2024.3403911.

Digital Object Identifier 10.1109/TMECH.2024.3403911

by a natural disaster). As a result, UAVs employed in such missions need to be equipped with wireless devices to establish on-demand communication among the UAVs without ground infrastructure support [2]. Considering the long distances between the UAVs, the directional antennas have gained attention for wireless communication due to their lower interference with neighbors and extended transmission range compared to their omnidirectional counterparts [3], [4], [5]. As the UAVs serve as the network nodes, the fast alterations in their relative positions make the UAV network distinct from many other wireless networks on the ground [6].

A directional antenna pair provides long-range communication when the antennas are aligned [7]. In a scenario where two moving UAVs are equipped with directional antennas for point-to-point communication, maintaining high-performance communication requires continuous adjustment of antenna orientations. While real-time global positioning system (GPS) data can be utilized to calculate the best orientation (e.g., see [8]), there are two associated problems. First, achieving high precision requires expensive GPS equipment, posing economic challenges for widespread deployment [9]. Second, the GPS signal may be lost due to wireless disturbances, blockages, and denied environments. Furthermore, in general, it is not available in indoor settings [10].

The observations above highlight the opportunities for utilizing a received signal strength indicator (RSSI)-based approach to the directional antenna pair alignment problem. In [11], a pattern-based search algorithm finds the best orientation that maximizes the RSSI signal. In [12] and [13], an algorithm based on an unscented Kalman filter and fuzzy logic utilizes the combined GPS and RSSI data to estimate the best orientation. In [14], RSSI measurement is utilized for an initial scan; however, the tracking of the best orientation is performed using GPS data. In [15] and [16], reinforcement learning-based algorithms learn the communication channel model parameters to estimate the best orientation. However, to the best of the authors' knowledge, literature lacks a pure control-theoretic approach to the problem.

#### B. Contribution

This article considers the alignment of the directional antenna pairs in UAV communication. In particular, two UAVs are equipped with directional antennas for point-to-point communication. We assume that each directional antenna has a 1-degree

1083-4435 © 2024 IEEE. Personal use is permitted, but republication/redistribution requires IEEE permission. See https://www.ieee.org/publications/rights/index.html for more information.



Fig. 1. Directional antenna with its 1-DOF rotating platform installed on a quadrotor UAV. The propeller blades are folded in the photo.

of freedom (DOF) rotating platform component to adjust its orientation (see Fig. 1). The control problem addressed herein is achieving convergence to the best orientation when the UAVs are stationary, as well as tracking the best orientation with an error during motion. From a control theory point of view, this problem is similar to the leader-following consensus problems of second-order multiagent systems where two directional antennas are the agents and the best orientation is the leader. From this perspective, we propose a nonlinear distributed static state feedback control law to solve the directional antenna pair alignment problem. The contributions of this article are outlined as follows.

No GPS Data are Required. RSSI Data are Utilized for Tracking Error Measurement: Distributed static state feedback control laws (e.g., see [17]) to solve leader-following consensus problems require a subset of the agents to access the relative tracking error (i.e., the distance to their neighboring agents) and a subset of the agents to access the tracking error (i.e., the distance to the leader). In the directional antenna pair alignment problem, directional antennas can exchange their orientation information via the communication channel to compute the relative tracking error (i.e., the angle between the directional antennas). However, without the GPS data, existing literature lacks a method to measure the tracking error (i.e., the angle between the best orientation and the directional antenna). Given the cosine beam model in [18], the partial derivative of the RSSI data with respect to the directional antenna orientation is a trigonometric function of the tracking error. This article proposes a distributed control law that relies on this property of the RSSI model, enabling directional antennas to access the tracking error.

Analysis of Problem Solvability: The closed-loop system incorporates nonlinear terms, resulting in infinitely many equilibrium points. We propose four conditions for selecting control gains that eliminate the existence of all equilibrium points except for the best and worst orientations. Moreover, under these proposed conditions, we show that the best orientation is asymptotically stable, whereas the worst orientation is unstable. The main theorem of this article shows that the overall closed-loop system converges to the best orientation for almost all initial states.

Practical Implementation Guidance: Approximating the partial derivative of RSSI with respect to the directional antenna

orientation requires RSSI measurements for various directional antenna orientations. However, it may become impossible if the directional antenna orientation does not change much for a time interval. To overcome this, we propose a swinging algorithm for one of the directional antennas. This algorithm induces a small perturbation around the current orientation of the directional antenna, while the nonlinear distributed static state feedback control law solves the alignment problem. This small perturbation creates a stereo effect (similar to having two directional antennas on the same UAV with an orientation offset). Consequently, one of the directional antennas can approximate the partial derivative term and gain access to the tracking error.

Experimental Validation: To demonstrate the effectiveness, we implement the proposed control law in a setup consisting of two UAVs equipped with directional antennas. The experiment focuses on a scenario where one UAV hovers above the ground station while the second UAV flies in a remote area.

# C. Notation

We write " $\equiv$ " to denote congruence modulo and  $\operatorname{atan2}(y,x)$  to denote 2-argument arctangent. The function  $\mathrm{N}:\mathbb{R}\to(-\pi,\pi]$  computes the principal value of an angle and is defined as  $\mathrm{N}(x)=\operatorname{atan2}(\sin(x),\cos(x))$ . For any  $\theta_1,\theta_2\in\mathbb{R}$  to be normalized, the principal value function has the properties: 1)  $\mathrm{N}(-\theta_1)=-\mathrm{N}(\theta_1),2)\,\mathrm{N}(\theta_1)=\mathrm{N}(\theta_1+2k\pi)$  for all  $k\in\mathbb{Z}$ , and 3)  $\mathrm{N}(\mathrm{N}(\theta_1)+\mathrm{N}(\theta_2))=\mathrm{N}(\theta_1+\theta_2)$ .

# II. PROBLEM FORMULATION

Consider a pair of UAVs: Let their location in 3-D space be  $(x_i(t),y_i(t),z_i(t))$  and the roll, pitch, and yaw angles describing their orientation be  $(\phi_i(t),\theta_i(t),\psi_i(t))$  (ZYX Euler angles). Each UAV carries a directional antenna to communicate with the other one. Each antenna has a 1-DOF rotating platform component to adjust its yaw angle. This capability allows directional antennas to orient themselves toward each other for a robust and reliable connection. Therefore, the location and orientation of the directional antennas are the ones of their corresponding UAVs, except the yaw angle. In other words, the location of the ith antenna is  $(x_i(t),y_i(t),z_i(t))$  and the roll, pitch, and yaw angles describing its orientation are  $(\phi_i(t),\theta_i(t),\alpha_i(t))$  (ZYX Euler angles). The mechanical dynamics of the 1-DOF rotating platform components of the directional antennas are

$$\dot{\alpha}_i(t) = \frac{\cos(\phi_i(t))}{\cos(\theta_i(t))} w_i(t) + \dot{\psi}_i(t)$$
 (1a)

$$\dot{w}_i(t) = -aw_i(t) + bu_i(t) \tag{1b}$$

where  $w_i(t) \in \mathbb{R}$  is the angular velocity,  $u_i(t) \in \mathbb{R}$  is the control input,  $a \geq 0$  is the ratio of viscous friction to moment of inertia, and b > 0 is the ratio of torque to input voltage times moment of inertia for the *i*th directional antenna for  $i \in \{1,2\}$ . Note that  $w_i(t)$  is the angular velocity of the rotating platform component of the directional antenna with respect to the UAV; thus, it can be measured with an encoder on the motor of the rotating platform component or with inertial measurement units (IMUs) by computing the difference between the angular velocity of

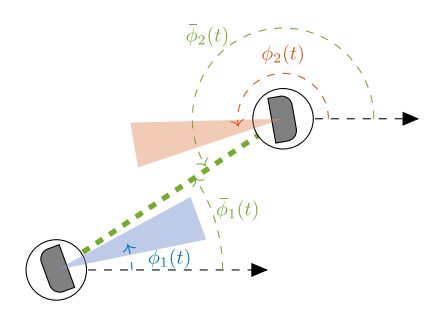


Fig. 2. Proposed nonlinear distributed static state feedback control law drives  $\alpha_1(t)$  toward  $\bar{\alpha}_1(t)$  and  $\alpha_2(t)$  toward  $\bar{\alpha}_2(t)$  for a better alignment.

the directional antenna and the angular velocity of the UAV in z-axis. Equation (1a) is the relationship between the angular velocities and Euler angle rates, where the UAV's yaw angle rate  $\dot{\psi}_i(t)$  can be considered as a disturbance.

Considering their locations, the distance between the directional antennas and the best orientations are given by

$$d(t) = \sqrt{(x_1 - x_2)^2 + (y_1 - y_2)^2 + (z_1 - z_2)^2}$$
 (2a)

$$\bar{\theta}_i(t) = -\text{atan2}\left(z_j - z_i, \sqrt{(x_j - x_i)^2 + (y_j - y_i)^2}\right)$$
 (2b)

$$\bar{\alpha}_i(t) = \operatorname{atan2}(y_i(t) - y_i(t), x_i(t) - x_i(t)) \tag{2c}$$

for  $i, j \in \{1, 2\}$  and  $i \neq j$ , where  $\bar{\theta}_i(t)$  and  $\bar{\alpha}_i(t)$  are the best pitch and yaw angles that make the *i*th directional antenna to point toward the other one. Note that

$$\bar{\alpha}_1(t) \equiv \bar{\alpha}_2(t) + \pi \pmod{2\pi} \tag{3}$$

by the definition of atan2 function. The amplitude of the best pitch angle  $|\bar{\theta}_i(t)|$  is a small value when the UAVs fly at a distance with a bounded altitude offset, as can be seen in (2b). A proper altitude control can keep  $|z_1(t)-z_2(t)|$  within the range of the radiation beam width of the directional antenna. The control objective of the rotating platform components of the directional antennas is to drive the current yaw angles  $\alpha_i(t)$  of the directional antennas to their best orientations  $\bar{\alpha}_i(t)$  (see Fig. 2).

Each directional antenna functions both as a receiver and transmitter of data. The power  $P_{\mathrm{r}i}$  in the received signal at the ith antenna is affected by the distance between the directional antennas and their orientations, as modeled in the Friis transmission equation. In particular, the RSSI level at the ith directional antenna is given by

$$P_{ri}(t, \alpha_i, \alpha_j, \theta_i, \theta_j) = P_{tj} - 20 \log_{10} \left(\frac{4\pi d(t)}{\lambda}\right) + G_{tj}^{\min} + \left(G_{tj}^{\max} - G_{tj}^{\min}\right) G(\alpha_j(t) - \bar{\alpha}_j(t), \theta_j(t) - \bar{\theta}_j(t)) + G_{ri}^{\min} + \left(G_{ri}^{\max} - G_{ri}^{\min}\right) G(\alpha_i(t) - \bar{\alpha}_i(t), \theta_i(t) - \bar{\theta}_i(t))$$
(4)

for  $i, j \in \{1, 2\}$  and  $i \neq j$ , where  $P_{tj}$  is the transmitting output power of the jth antenna in decibels (dB),  $G_{tj}^{\min}$  and  $G_{tj}^{\max}$  are

transmitting gains of the jth antenna,  $G_{ri}^{\min}$  and  $G_{ri}^{\max}$  receiving gains of the ith antenna, and  $\lambda$  is the wavelength. Considering the simple 2-D cosine beam model for the agains (see [18]), the function  $G(\alpha, \theta) = \cos^{n_{\alpha}}(\alpha/2)\cos^{n_{\theta}}(\theta)$  is the amplitude pattern for which we consider  $n_{\alpha} = 2$  and  $n_{\theta} > 0$ . Let  $P_{ri}(t, \alpha_i, \alpha_j) = P_{ri}(t, \alpha_i, \alpha_j, 0, 0)$ .

Next, we define the RSSI-based directional antenna pair alignment problem.

Problem 1: Let the best orientations in (2) be unknown. For  $i \in \{1,2\}$  and  $t \geq 0$ , let the UAVs be stationary, i.e.,  $\phi_i(t) = 0$ ,  $\theta_i(t) = 0$ , and  $\dot{\psi}_i(t) = 0$ , and let them be at the same altitude, i.e.,  $z_1(t) = z_2(t)$ . Given the system in (1) together with the RSSI levels in (4), find a control law  $u_i$  for  $i \in \{1,2\}$  such that  $\lim_{t \to \infty} \alpha_i(t) \equiv \bar{\alpha}_i \pmod{2\pi}$  for almost all initial states of the closed-loop system.

Note that the distance and the best orientations in (2) are also stationary when the UAVs are stationary as in Problem 1. A follow-up problem here is the case where  $|\phi_i(t)| \leq \beta_1$ ,  $|\theta_i(t)| \leq \beta_1$ ,  $|\dot{\theta}_i(t)| \leq \beta_2$ ,  $|\dot{\theta}_i(t)| \leq \beta_2$ , and  $|\dot{\psi}_i(t)| \leq \beta_2$ ,  $|z_1(t)-z_2(t)| \leq \beta_3$ , and  $|\dot{z}_1(t)| \leq \beta_4$  and  $|\dot{z}_2(t)| \leq \beta_4$ , for  $t \geq 0$  and  $i \in \{1,2\}$ , where  $\beta_1 > 0$ ,  $\beta_2 > 0$ ,  $\beta_3 > 0$ , and  $\beta_4 > 0$ . For this case, the objective is to track the best orientation with a tracking error, i.e.,  $\lim_{t\to\infty} |\mathrm{N}(\alpha_i(t)-\bar{\alpha}_i(t))| \leq \epsilon$  for some  $\epsilon > 0$ .

#### III. DISTRIBUTED CONTROL LAW

Unless explicitly stated otherwise, we will assume that the UAVs are stationary and at the same altitude throughout the section.

## A. Design

In Problem 1,  $\bar{\alpha}_i(t)$  information is not available to the directional antennas. However,  $P_{\mathrm{r}i}(t,\alpha_i,\alpha_j)$  and  $\alpha_i(t)$  are available to the ith directional antenna. Furthermore, the directional antennas can exchange any information, including  $\alpha_j(t)$ . Based on the available information, we propose the control law

$$u_{i}(t) = -k_{d}w_{i}(t) - k_{ij}N(\alpha_{i}(t) - \alpha_{j}(t) + \pi) + g_{i}\frac{\partial P_{ri}(t, \alpha_{i}, \alpha_{j})}{\partial \alpha_{i}(t)}$$
(5)

for  $i, j \in \{1, 2\}, i \neq j$ , where  $k_{ij} \geq 0$ ,  $g_i \geq 0$ , and  $k_d \in \mathbb{R}$  are control gains. Note that the partial derivative term satisfies

$$\frac{\partial P_{\rm ri}(t,\alpha_i,\alpha_j)}{\partial \alpha_i(t)} = -\frac{(G_{\rm ri}^{\rm max} - G_{\rm ri}^{\rm min})}{2} \sin(\alpha_i(t) - \bar{\alpha}_i) \quad (6)$$

due to (4). Therefore, the control law in (5) is a nonlinear function of the states  $\alpha_i(t)$  and  $w_i(t)$ , making it a nonlinear distributed static state feedback control law.

<sup>&</sup>lt;sup>1</sup>The beam pattern of the directional antenna of our setup can be found in https://dl.ubnt.com/datasheets/nanostationm/nsm\_ds\_web.pdf.

 $<sup>^2 \</sup>text{The wavelength} \ \lambda = v/f, \ \text{where} \ v \ \text{is} \ \text{the phase speed of the wave} \ \text{and} \ f \ \text{is} \ \text{the frequency of the wave}. \ \text{In free space, the phase speed is equivalent to the speed of light, i.e.,} \ v \approx 3 \times 10^8. \ \text{Consequently, for Wi-Fi signals with a frequency of} \ f = 2.4 \ \text{GHz}, \ \text{the wavelength is} \ \lambda \approx 0.125 \ \text{m, and for Wi-Fi signals with a frequency of} \ f = 5 \ \text{GHz}, \ \text{the wavelength is} \ \lambda \approx 0.06 \ \text{m}.$ 







Fig. 3. Closed-loop system have an infinite number of isolated equilibrium points, with half representing the best orientation and the remaining half representing the worst orientation under Conditions 1 and 2. These conditions eliminate the existence of the equilibrium points with a different configuration.

For stationary UAVs as in Problem 1, the closed-loop system dynamics are given by

$$\dot{\alpha}_1(t) = w_1(t) \tag{7a}$$

$$\dot{\alpha}_2(t) = w_2(t) \tag{7b}$$

$$\dot{w}_1(t) = -(a+bk_d)w_1(t) - bk_{12}N(\alpha_1(t) - \alpha_2(t) + \pi) -$$

$$bq_1G_{\star 1}^{\text{med}}\sin(\alpha_1(t) - \bar{\alpha}_1) \tag{7c}$$

$$\dot{w}_2(t) = -(a + bk_d)w_2(t) - bk_{21}N(\alpha_2(t) - \alpha_1(t) + \pi)$$

$$bq_2G_{r2}^{\text{med}}\sin(\alpha_2(t) - \bar{\alpha}_2) \tag{7d}$$

from (1), (4), (5), and (6), where  $G_{\rm r}^{\rm med} = (G_{\rm r}^{\rm max} - G_{\rm r}^{\rm min})/2 > 0$ . The following conditions provide guidance on the control gains selection.

Condition 1: At least one of the following holds:

- 1)  $g_1 > 0$  and  $k_{21} > 0$ ;
- 2)  $g_2 > 0$  and  $k_{12} > 0$ .

Condition 2: The following holds:

$$k_{12}g_2G_{\rm r2}^{\rm med} + k_{21}g_1G_{\rm r1}^{\rm med} > g_1g_2G_{\rm r1}^{\rm med}G_{\rm r2}^{\rm med}$$

Condition 3: The following holds:  $a_c = a + bk_d > 0$ .

Condition 4: The following holds:  $k_{12} > 0$  and  $k_{21} > 0$ .

*Remark 1:* We listed Conditions 1, 2, and 4 separately because different theorems rely on different conditions. It is possible to combine and express them collectively. This combination yields that exactly one of the following three holds: 1)  $g_1 > 0$ ,  $g_2 = 0$ ,  $k_{21} > 0$ ,  $k_{12} > 0$ ; 2)  $g_1 = 0$ ,  $g_2 > 0$ ,  $k_{21} > 0$ ,  $k_{12} > 0$ ; 3)  $g_1 > 0$ ,  $g_2 > 0$ ,  $k_{21} > 0$ ,  $k_{12} > 0$  such that  $k_{12}g_2G_{\rm re}^{\rm med} + k_{21}g_1G_{\rm rl}^{\rm med} > g_1g_2G_{\rm rl}^{\rm med}G_{\rm r2}^{\rm med}$ .

*Remark 2:* We can consider the best orientations  $\bar{\alpha}_1$  and  $\bar{\alpha}_2$  as the outputs of an exosystem. Considering the two directional antennas as agents and the exosystem as a leader node, we can form a graph  $\bar{\mathcal{G}}$  with three nodes linked by edges  $k_{ij}$  and pinning gains  $g_i$ . A standard assumption in the leader-following consensus problems of the multiagent systems is that  $\bar{\mathcal{G}}$  contains a directed spanning tree (see [17]). Condition 1 guarantees the existence of a directed spanning tree. Condition 2 is nonstandard. The reason behind this condition is the nonlinear nature of the closed-loop system in (7). The closed-loop system in (7) has infinitely many isolated equilibrium points that may lead to convergence to a configuration other than the best orientation. Lemma 1 shows that Conditions 1 and 2 ensure the absence of equilibrium points except for the best and worst orientations, as illustrated in Fig. 3. Condition 3 is necessary for the asymptotic stability of the best orientation in Lemma 2 as a result of Lemma 1 in [17]. Finally, Theorem 1 relies on Condition 4 to construct a Lyapunov function to prove the solvability of Problem 1. It is an open

problem if the Lyapunov function in Theorem 1 can be replaced to avoid this condition.

## B. Solvability Analysis of Problem 1

The following lemma shows that there is no equilibrium point except the two configurations illustrated in Fig. 3 under Conditions 1 and 2.

*Lemma 1:* Let Conditions 1 and 2 hold. An equilibrium point  $(\alpha_1^*, \alpha_2^*, w_1^*, w_2^*)$  of the closed-loop system in (7) either represents the best orientation

$$\alpha_1^* \equiv \bar{\alpha}_1 \pmod{2\pi}, \quad \alpha_2^* \equiv \bar{\alpha}_1 + \pi \pmod{2\pi}$$
 (8)

or the worst orientation

$$\alpha_1^* \equiv \bar{\alpha}_1 + \pi \pmod{2\pi}, \quad \alpha_2^* \equiv \bar{\alpha}_1 \pmod{2\pi}$$
 (9)

where  $w_1^* = w_2^* = 0$ .

*Proof:* After applying the two properties mentioned in Section I-C, we find  $N(\alpha_2^* - \alpha_1^* + \pi) = -N(\alpha_1^* - \alpha_2^* + \pi)$ . Trivially,  $w_1^* = w_2^* = 0$  from (7a) and (7b). Since the proof for the item (2) follows the same derivation, we only present the proof for the item (1) of Condition 1 by separating it into the following subitems.

- 1a)  $g_1 > 0$  and  $k_{21} > 0$  and  $g_2 = 0$  and  $k_{12} \ge 0$
- 1b)  $g_1 > 0$  and  $k_{21} > 0$  and  $g_2 > 0$  and  $k_{12} = 0$
- 1c)  $g_1 > 0$  and  $k_{21} > 0$  and  $g_2 > 0$  and  $k_{12} > 0$
- 1a) We have  $N(\alpha_2^* \alpha_1^* + \pi) = -N(\alpha_1^* \alpha_2^* + \pi) = 0$  from (7d). Therefore,  $\sin(\alpha_1^* \bar{\alpha}_1) = 0$  from (7c), resulting in two sets of solutions  $\alpha_1^* \equiv \bar{\alpha}_1 \pmod{2\pi}$  and  $\alpha_1^* \equiv \bar{\alpha}_1 + \pi \pmod{2\pi}$ . Combining this with  $N(\alpha_2^* \alpha_1^* + \pi) = 0$  yield (8) and (9).

1b) We have  $\sin(\alpha_1^* - \bar{\alpha}_1) = 0$  from (7c), resulting in two sets of solutions  $\alpha_1^* \equiv \bar{\alpha}_1 \pmod{2\pi}$  and  $\alpha_1^* \equiv \bar{\alpha}_1 + \pi \pmod{2\pi}$ . For  $\alpha_1^* \equiv \bar{\alpha}_1 \pmod{2\pi}$ , we have

$$-k_{21}N(\alpha_2^* - \bar{\alpha}_1 + \pi) - g_2G_{r2}^{\text{med}}\sin(\alpha_2^* - \bar{\alpha}_1 + \pi) = 0$$

from (7d). The only solution is the trivial one  $\alpha_2^* \equiv \bar{\alpha}_1 + \pi \pmod{2\pi}$  from Lemma 3 since  $c = -k_{21/g_2}G_{\rm r2}^{\rm med} < 0$ . This yields the best orientation in (8). For  $\alpha_1^* \equiv \bar{\alpha}_1 + \pi \pmod{2\pi}$ , we have

$$k_{21}N(\alpha_2^* - \bar{\alpha}_1) - g_2G_{r_2}^{\text{med}}\sin(\alpha_2^* - \bar{\alpha}_1) = 0$$

from (7d) and the fact that  $\sin(\alpha_2^* - \bar{\alpha}_1 + \pi) = -\sin(\alpha_2^* - \bar{\alpha}_1)$ . The only solution is the trivial one  $\alpha_2^* \equiv \bar{\alpha}_1 \pmod{2\pi}$  from Lemma 3 since  $c = k_{21}/g_2 G_{r2}^{\text{med}} \geq 1$  from Condition 2. This yields the worst orientation in (9).

1c) Equations (7c) and (7d) yields

$$-\frac{k_{12}}{g_1 G_{r1}^{\text{med}}} N(\alpha_1^* - \alpha_2^* + \pi) - \sin(\alpha_1^* - \bar{\alpha}_1) = 0 \quad (10a)$$

$$-\frac{k_{21}}{g_2 G_{\rm r2}^{\rm med}} N(\alpha_2^* - \alpha_1^* + \pi) - \sin(\alpha_2^* - \bar{\alpha}_1 + \pi) = 0. \quad (10b)$$

There exists no solution to (10) except the ones in (8) and (9) from Lemma 4 with  $c_1 = -k_{12}/g_1G_{\rm r1}^{\rm med}$ ,  $c_2 = k_{21}/g_2G_{\rm r2}^{\rm med}$ ,  $\theta_1 = \alpha_1^* - \bar{\alpha}_1$ , and  $\theta_2 = \alpha_2^* - \bar{\alpha}_1 + \pi$ , since  $|c_1 - c_2| \ge 1$  from Condition 2.

The following lemma determines the types of the equilibrium points in (8) and (9).

Lemma 2: Let Conditions 1–3 hold. The equilibrium points specified in (8) are asymptotically stable, whereas those in (9) are unstable.

*Proof:* To represent the closed-loop system in a compact form, we define the following matrices:

$$\mathcal{L} = \begin{bmatrix} k_{12} & -k_{12} \\ -k_{21} & k_{21} \end{bmatrix}, \quad \mathcal{G} = \begin{bmatrix} G_{\mathrm{r}1}^{\mathrm{med}} g_1 & 0 \\ 0 & G_{\mathrm{r}2}^{\mathrm{med}} g_2 \end{bmatrix}.$$

The linearization of the closed-loop system in (5) at the best orientation in (8) and the worst orientation in (9), respectively, yields the system matrices

$$A_{\rm gb} = \begin{bmatrix} 0 & I_2 \\ -b(\mathcal{L} + \mathcal{G}) & -a_{\rm c}I_2 \end{bmatrix}$$
 (11a)

$$A_{gw} = \begin{bmatrix} 0 & I_2 \\ -b(\mathcal{L} - \mathcal{G}) & -a_c I_2 \end{bmatrix}. \tag{11b}$$

"Best orientation is asymptotically stable" Part: Let  $\lambda_1$  and  $\lambda_2 \in \mathbb{C}$  be the eigenvalues of  $\mathcal{L} + \mathcal{G}$ . Its characteristic equation given by

$$\det(sI_2 - (\mathcal{L} + \mathcal{G})) = s^2 + p_{b1}s + p_{b0} = (s - \lambda_1)(s - \lambda_2)$$

is a quadratic equation with the coefficients given by

$$\begin{split} p_{\rm b1} &= -k_{12} - k_{21} - g_1 G_{\rm r1}^{\rm med} - g_2 G_{\rm r2}^{\rm med} \\ p_{\rm b0} &= g_1 G_{\rm r1}^{\rm med} g_2 G_{\rm r2}^{\rm med} + k_{21} g_1 G_{\rm r1}^{\rm med} + k_{12} g_2 G_{\rm r2}^{\rm med} \end{split}$$

We deduce that  $\lambda_1$  and  $\lambda_2$  are real numbers since the discriminant of the quadratic equation satisfies

$$\begin{aligned} p_{\text{b1}}^2 - 4p_{\text{b0}} \\ &= \left(k_{12} - k_{21} + g_1 G_{\text{r1}}^{\text{med}} - g_2 G_{\text{r2}}^{\text{med}}\right)^2 + 4k_{12}k_{21} \ge 0. \end{aligned}$$

The coefficient  $p_{\rm b0}>0$  under Condition 1. Since the eigenvalues satisfy  $\lambda_1\lambda_2=p_{\rm b0}>0$  and  $\lambda_1+\lambda_2=-p_{\rm b1}>0$ , we conclude that  $\lambda_1>0$  and  $\lambda_2>0$ . Now, the characteristic equation of  $A_{\rm gb}$  is given by

$$\det(sI_4 - A_{gb}) = s^2 I_2 + sa_c I_2 + b(\mathcal{L} + \mathcal{G})$$
  
=  $(s^2 + sa_c + b\lambda_1)(s^2 + sa_c + b\lambda_2)$ 

the roots of which have negative real parts since  $a_c > 0$  from Condition 3,  $b\lambda_1 > 0$ , and  $b\lambda_2 > 0$ .

"Worst orientation is unstable" Part: Let  $\mu_1$  and  $\mu_2 \in \mathbb{C}$  be the eigenvalues of  $\mathcal{L} - \mathcal{G}$ . Its characteristic equation

$$\det(sI_2 - (\mathcal{L} - \mathcal{G})) = s^2 + p_{w1}s + p_{w0} = (s - \mu_1)(s - \mu_2)$$

is a quadratic one with the coefficients given by

$$p_{w1} = -k_{12} - k_{21} + g_1 G_{r1}^{\text{med}} + g_2 G_{r2}^{\text{med}}$$

$$p_{w0} = g_1 G_{r1}^{\text{med}} g_2 G_{r2}^{\text{med}} - k_{21} g_1 G_{r1}^{\text{med}} - k_{12} g_2 G_{r2}^{\text{med}}.$$

We deduce that  $\mu_1$  and  $\mu_2$  are real numbers since the discriminant of the quadratic equation satisfies

$$p_{\text{w}1}^2 - 4p_{\text{w}0} = (k_{12} - k_{21} - g_1 G_{\text{r}1}^{\text{med}} + g_2 G_{\text{r}2}^{\text{med}})^2 + 4k_{12}k_{21} \ge 0.$$

The coefficient  $p_{\rm w0}<0$  from Condition 2. Therefore,  $\mu_1\mu_2=p_{\rm w0}<0$ . Without loss of generality, we conclude that  $\mu_1<0$ . Now, the characteristic equation of  $A_{\rm gw}$  is given by

$$\det(sI_4 - A_{gw}) = s^2 I_2 + sa_c I_2 + b(\mathcal{L} - \mathcal{G})$$
  
=  $(s^2 + sa_c + b\mu_1) (s^2 + sa_c + b\mu_2)$ .

There exists a positive root of  $s^2 + sa_c + b\mu_1$  since  $a_c > 0$  and  $\mu_1 < 0$ .

The next theorem investigates the solvability of Problem 1.

Theorem 1: Let Conditions 1–4 hold. The nonlinear distributed static state feedback control law in (5) solves the RSSI-based directional antenna pair alignment problem defined in Problem 1.

*Proof:* Let  $\tilde{\alpha}_1(t) = \mathrm{N}(\alpha_1(t) - \bar{\alpha}_1)$  and  $\tilde{\alpha}_2(t) = \mathrm{N}(\alpha_2(t) - \bar{\alpha}_1 + \pi)$  for which  $\dot{\tilde{\alpha}}_1(t) = w_1(t)$  and  $\dot{\tilde{\alpha}}_2(t) = w_2(t)$  almost everywhere. Consider the following Lyapunov function:

$$V(t) = k_{21}w_1^2 + k_{12}w_2^2 + bk_{12}k_{21}N^2(\tilde{\alpha}_1(t) - \tilde{\alpha}_2(t))$$
$$+ 2bg_1G_{r1}^{\text{med}}k_{21}(1 - \cos(\tilde{\alpha}_1(t)))$$
$$+ 2bg_2G_{r2}^{\text{med}}k_{12}(1 - \cos(\tilde{\alpha}_2(t))).$$

Note that  $N^2(\cdot)$  and V(t) are continuous functions. Under Conditions 1–4, the derivative of the Lyapunov function is negative semidefinite, i.e.,  $\dot{V}(t) = -2a_c e_{21} w_1^2(t) - 2a_c e_{12} w_2^2(t) \leq 0$  for all  $w_1(t), w_2(t), \tilde{\alpha}_1(t), \tilde{\alpha}_2(t) \in \mathbb{R}$ . Let

$$\bar{V} = k_{21}w_1^2(0) + k_{12}w_1^2(0) + 2bk_{12}k_{21}\pi^2$$

$$+ 4bg_1G_{r1}^{\text{med}}k_{21} + 4bg_2G_{r2}^{\text{med}}k_{12}$$

for which  $V(t) \leq \bar{V}$  for all  $t \geq 0$ .

We prove the theorem by the invariance principle. We have  $|\tilde{\alpha}_i(t)| \leq \pi$  for all  $t \geq 0$  due to  $\mathrm{N}(\cdot)$  function. We also have  $|w_i| \leq \bar{V}/k_{ij}$  for all  $t \geq 0$  since  $V(t) \leq \bar{V}$ . Therefore, the compact set

$$\Omega = \{ (\tilde{\alpha}_1, \tilde{\alpha}_2, w_1, w_2) \mid |\tilde{\alpha}_i| \le \pi, |w_i| \le \bar{V}/k_{ij}, i \in \{1, 2\} \}$$

is positively invariant with respect to (7). Let

$$E = \left\{ \tilde{\alpha}_1, \tilde{\alpha}_2, w_1, w_2 \mid \dot{V} = 0 \right\}$$
  
=  $\{ w_1, w_2, \tilde{\alpha}_1, \tilde{\alpha}_2 \mid (w_1, w_2) = (0, 0) \}$ 

be all the points in  $\Omega$ , where  $\dot{V}=0$ . Finally, the set  $M=\{(0,0,0,0),(\pi,\pi,0,0)\}$  is the largest invariant set in E from (7c) and (7d). Then, every solution starts in  $\Omega$  approaches M as  $t\to\infty$  from LaSalle's theorem (e.g., see [19, Th. 4.4]). Since  $\Omega$  is compact and positively invariant for any initial state  $w_1(0), w_2(0), \tilde{\alpha}_1(0), \tilde{\alpha}_2(0)$ , every solution converges to either the best orientation in (8) or the worst orientation in (9) for all initial states. From the central manifold theorem (see [20, Th. 3.2.1]), there exists a nontrivial unstable manifold of the equilibrium point in (9); therefore, its stable manifold has a dimension lower than  $\mathbb{R}^4$ . We conclude that the solution converges to the best orientation for almost all initial states.

For UAVs in motion, (7) corresponds to the linearization of the dynamics in (1), (4), and (5) at the hover state at the same altitude. By linearization and an input-to-state stability argument, it can

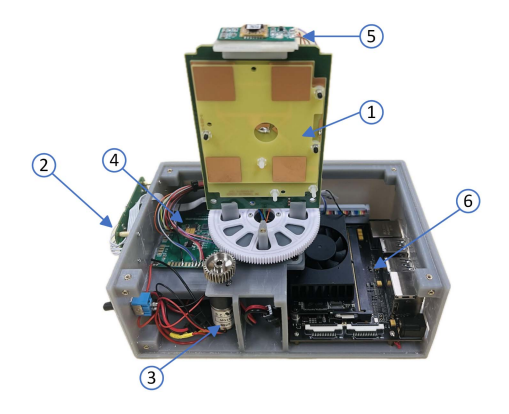


Fig. 4. Hardware overview. ① directional antenna. ② WiFi router. ③ DC motor. ④ Motor driver. ⑤ IMU. ⑥ Computation module.

be shown that the directional antennas track their best orientation for the follow-up problem below Problem 1 for sufficiently small  $\beta_1$ ,  $\beta_2$ ,  $\beta_3$ , and  $\beta_4$ .

# IV. EXPERIMENTAL RESULTS

To demonstrate the efficacy of the nonlinear distributed control law in (5) for solving Problem 1, we conducted an experiment involving two UAVs equipped with two directional antennas. The experiment specifically focused on a scenario where one UAV hovers above the ground station and the other one flies in a remote area. We refer to the directional antenna of the stationary UAV as the *local system* and the directional antenna of the mobile UAV as the *remote system*.

## A. System Hardware Design

An overview of our hardware design is shown in Fig. 4. As seen in the figure, each directional antenna has a rotating platform component to adjust its orientation.

The communication module has a Ubiquiti Nanostation Loco M5 directional antenna and a TP-Link TL-WR902AC WiFi router. The directional antenna (① in Fig. 4) is installed on a lazy Susan connected to a 140-tooth gear, which allows 1-DOF rotation. Ubiquiti Nanostation Loco M5 is chosen due to its overall performance and Linux-based Air operating system (OS). The Air OS provides the common network interface to access the RSSI data, which avoids kernel-level and hardware modification. The WiFi router (② in Fig 4) establishes the data transfer between the directional antenna, the computation module, and the ground station. The TP-Link TL-WR902AC is utilized for its compact size (74  $\times$  67  $\times$  22 mm) and low power consumption (2 watts).

Actuation is provided by a Nidec MG16B-030-AA-00 brushed dc geared motor (③ in Fig. 4). A planetary gearhead with a ratio of 30:1 is attached to generate the torque required to rotate the directional antennas. This motor can be powered by a rated voltage of 6 V with an angular velocity of 380 r/min and a max torque of 30 mN  $\cdot$  m. A 32-tooth gear is installed on top of the gearhead to rotate the antenna. The half-bridge Texas Instruments DRV8837 is used to drive the motor (④) in Fig. 4).

To implement the proposed control law, three types of sensor data are required, which are the yaw angle and the angular velocity of the directional antenna, and the RSSI. The RSSI can be accessed by simply using the network interface in Air OS. For the yaw angle and angular velocity, we choose the nine-axis IMU Xsens MTi-3 (⑤ in Fig. 4) with attitude and heading reference system (AHRS) feature. The AHRS feature can provide a true-north-referenced heading angle, which makes both subsystems utilize the same reference frame for the heading angle.

We select the Nvidia Xavier NX development kit (Xaiver) as the computation module (6 in Fig. 4). Xavier has a GPU, a 6-core CPU, and 40-pin general-purpose input/output (GPIO) including inter-integrated circuit (I2C), universal asynchronous receiver-transmitter (UART), pulse-width modulation (PWM) channel, etc. Xavier is sufficient not only for the control law computation but also for the emergency site video processing illustrated in [15]. Moreover, Xavier offers the potential to enhance UAV automation as a companion computer. The 40-pin GPIO enables the Xavier to utilize two PWM channels to the motor control speed and direction, the I2C port to achieve IMU data, and the UART port to read the RSSI data.

## B. System Identification

To determine the parameters a and b in (1b), we perform open-loop experiments by applying a pseudo-random binary signal (PRBS) as inputs to the rotating platform components. For additional information on PRBS signals and system identification methods, please see [21]. The Matlab System Identification Toolbox analyzed the inputs and resulting states of the experiments and it estimated the parameters as a = 6.00 and b = 19.69.

## C. Controller Implementation

The proposed control law in (5) relies on  $\partial P_{\mathrm{r}i}/\partial \alpha_i$  which is mathematically defined as

$$\frac{\partial P_{\mathrm{r}i}(t,\alpha_i,\alpha_j)}{\partial \alpha_i(t)} = \lim_{h \to 0} \frac{P_{\mathrm{r}i}(t,\alpha_i+h,\alpha_j) - P_{\mathrm{r}i}(t,\alpha_i-h,\alpha_j)}{2\,h}.$$

If there are two directional antennas on the same UAV with a small orientation offset (e.g.,  $h=5^{\circ}$ ), this partial derivative can be approximated by comparing the current RSSI levels at two different orientations. This does not apply to our setup since each UAV has one directional antenna.

First, we set  $g_2=0$  to not use  $\partial P_{\rm r2}/\partial \alpha_2$ . Still, we need to approximate  $\partial P_{\rm r1}/\partial \alpha_1$  due to Condition 1. We propose the following approximation:

$$\frac{\partial P_{\rm r}i(t,\alpha_i,\alpha_j)}{\partial \alpha_i(t)} \approx \frac{P_{\rm r}i(t,\alpha_i,\alpha_j) - P_{\rm r}i(t-T_1,\alpha_i,\alpha_j)}{\alpha_i(t) - \alpha_i(t-T_1)} \tag{12}$$

for some sampling interval  $T_1 > 0$ . However, this approximation can lead to division by zero issues due to the term  $\alpha_i(t) - \alpha_i(t - T_1)$ , especially if the orientation  $\alpha_i(t)$  has not changed significantly recently. To prevent division by zero, we perturb  $\alpha_1(t)$  with a square wave r(t). This perturbation creates

a stereo effect, similar to having two directional antennas on the local system.

However, exchanging a perturbed orientation  $\alpha_1(t)$  with the remote system would induce a perturbation on  $\alpha_2(t)$  as well. Therefore, we introduce a virtual system with the dynamics given by

$$\dot{\alpha}_{v1}(t) = w_{v1}(t),\tag{13a}$$

$$\dot{w}_{v1}(t) = -aw_{v1}(t) + bu_{v1}(t) \tag{13b}$$

where  $\alpha_{v1}(t) \in \mathbb{R}$  is the virtual orientation and  $w_{v1}(t) \in \mathbb{R}$  is the virtual angular velocity. The local one simulates the dynamics in (13) to perform the directional antenna pair alignment goal by utilizing the virtual control law given by

$$u_{v1}(t) = -k_{d}w_{v1}(t) - k_{12}N(\alpha_{v1}(t) - \alpha_{2}(t) + \pi) + g_{1}\frac{\partial P_{ri}(t, \alpha_{i}, \alpha_{j})}{\partial \alpha_{i}(t)}$$

$$(14)$$

where the partial derivative term is approximated using (12). Consequently, the exchange of any perturbed state information is prevented. Now, a PD controller given by

$$u_{1}(t) = -k_{d1}(w_{1}(t) - w_{v1}(t))$$
$$-k_{p1}N(\alpha_{1}(t) - \alpha_{v1}(t) - r(t))$$
(15)

makes  $\alpha_1(t)$  track  $\alpha_{v1}(t)+r(t)$  to perturb around the virtual orientation, where  $k_{p1}>0$  and  $k_{d1}\in\mathbb{R}$  are the control gains. The remote system incorporates the virtual orientation of the local system into its control law, given by

$$u_2(t) = -k_{\rm d}w_2(t) - k_{21}N(\alpha_2(t) - \alpha_{\rm v1}(t) + \pi)$$
 (16)

to avoid the perturbations caused by r(t).

To implement the control law and information exchange between the two subsystems, a system architecture with Robot Operating System 2 (ROS2) is designed; see Fig. 5 for the software overview of the system. ROS2 is employed as a middleware to orchestrate the real-time communication between the local and the remote system. The control laws in (14)–(16) are implemented with a control frequency of 50 Hz. The control gains are set to  $k_d = 0.01$ ,  $k_{12} = 1$ ,  $k_{21} = 1$ ,  $g_1 = 2$ ,  $g_2 = 0$ ,  $k_{\rm p1}=1$ , and  $k_{\rm d1}=0.01$ . For these control parameters, Conditions 1–4 hold. The period of the square wave r(t) is set to  $T_1 = 0.5$  s, matching the sampling period of the approximator in (12). In other words, the update rate of the approximator is 2 Hz. The amplitude of the square wave r(t) should be adjusted considering the distance between the local and the remote systems. Close distances require higher perturbations since  $P_{\rm r1}$  does not vary much with a small perturbation at a close distance. As the distance between the systems increases, a small perturbation is sufficient. We set an amplitude of 20° for the experiment that we conducted at a distance range between 30-50 m.

# D. Test Result

We experimented with an outdoor setting. The local UAV is hovering while the remote one flies around at a distance of about 40 m from the local UAV, as shown in Fig. 6. Each

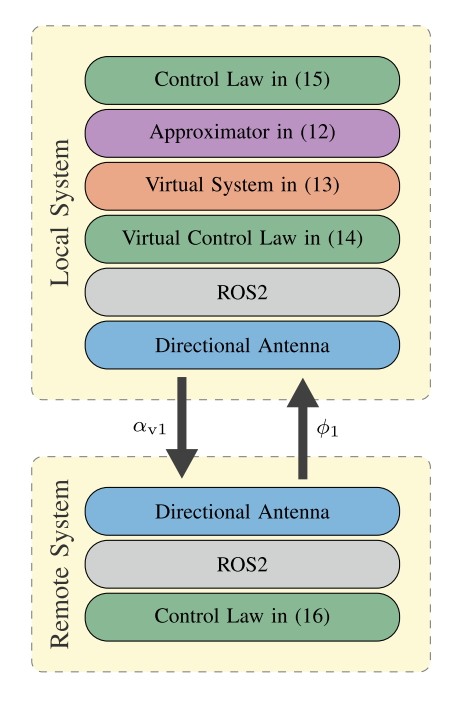


Fig. 5. Software overview.



Fig. 6. Outdoor setting where the experiment is conducted.

system is equipped with a UBLOX NEO M8N GPS module to estimate the best orientation to compare the performance of the proposed method. The experimental results in Fig. 7 show that both directional antennas track the best orientation with a small error. The swinging algorithm induces a small perturbation on the orientation  $\alpha_1$  around the virtual orientation  $\alpha_{v1}$  to approximate  $\partial P_{r1}/\partial \alpha_1$ .

### V. CONCLUSION

The experimental case study shows that the RSSI-based nonlinear static state feedback control law in (5) offers an efficient solution to the directional antenna pair alignment problem for scenarios where a GPS signal is unavailable. Conducting additional experiments to explore potential real-world application challenges is a future work. Another future work is the

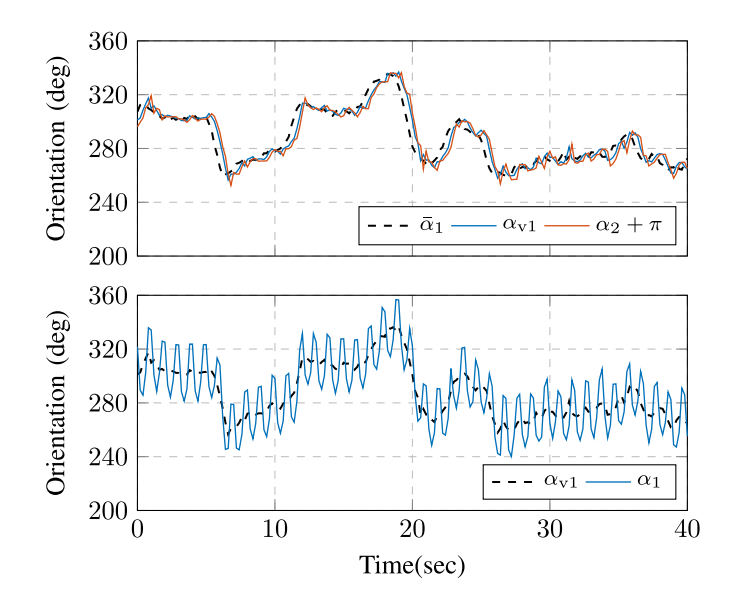


Fig. 7. Experimental results show that the virtual orientation  $\alpha_{v1}$  and orientation  $\alpha_2$  track the best orientation with an error.

development of intelligent swinging algorithms. For example, the amplitude of the square wave r(t) could be time-varying, allowing it to be set to zero when the system is already in motion, i.e.,  $|w_1(t)| > \epsilon$  for a threshold value  $\epsilon > 0$ . Another future work is the 2-DOF adjustment of the directional antennas, where they can also adjust their pitch angles independently.

### **APPENDIX**

This appendix investigates the existence of solutions for a set of nonlinear equations. The proofs presented in this section rely on a property of the *sinc function* given by

$$|\sin(\theta)/\theta| < 1, \quad \theta \neq 0 \tag{17}$$

which is well known in mathematical literature.

Lemma 3: Let  $c \notin [0,1)$ . The nonlinear equation  $cN(\theta) - \sin(\theta) = 0$  has no real solution except trivial solutions  $\theta \equiv 0 \pmod{2\pi}$ .

*Proof:* Assume there exists a nontrivial solution  $\theta^*$  (i.e.,  $N(\theta^*) \neq 0$ ). Without loss of generality, let  $\theta^* \in (-\pi, \pi] \setminus \{0\}$ . This restriction does not lead to a loss of generality because both  $N(\theta)$  and  $\sin(\theta)$  are periodic with period  $2\pi$ . Within this range,  $\sin(\theta^*)$  and  $\theta^*$  has the same sign; therefore, we deduce that  $0 \leq \sin(\theta^*)/\theta^* < 1$  from (17). However, it contradicts with the fact that  $\sin(\theta^*)/N(\theta^*) = c$  since  $c \notin [0,1)$ .

Lemma 4: Let  $|c_1 - c_2| \ge 1$ . The set of nonlinear equations

$$c_1 N(\theta_1 - \theta_2) - \sin(\theta_1) = 0$$
 (18a)

$$c_2 N(\theta_1 - \theta_2) - \sin(\theta_2) = 0$$
 (18b)

has no real solution except trivial solutions

$$(\theta_1, \theta_2) \equiv (0 \pmod{2\pi}, 0 \pmod{2\pi})$$
  
$$(\theta_1, \theta_2) \equiv (\pi \pmod{2\pi}, \pi \pmod{2\pi}).$$

We first provide two preliminary facts and their proofs before presenting the proof of this lemma.

Fact 1: Let  $\theta_1 - \theta_2 \neq 0$ . The inequality

$$-1 < \frac{\sin(\theta_1) - \sin(\theta_2)}{\theta_1 - \theta_2} < 1 \tag{19}$$

holds.

*Proof of Fact 1:* Let  $\psi = (\theta_1 + \theta_2)/2$  and  $h = (\theta_1 - \theta_2)/2$ , where  $h \neq 0$ . We can rewrite the function in (19) as  $(\sin(\psi + h) - \sin(\psi - h))/2h$ , that is inequivalent to  $\cos(\psi)\sin(h)/h$  after applying trigonometric sum identities. Note that  $|\cos(\psi)\sin(h)/h| \leq |\sin(h)/h| < 1$  for all  $h \in \mathbb{R} \setminus \{0\}$  from (17).

Fact 2: Let  $N(\theta_1 - \theta_2) \neq 0$ . The inequality

$$-1 < \frac{\sin(\theta_1) - \sin(\theta_2)}{N(\theta_1 - \theta_2)} < 1 \tag{20}$$

holds.

*Proof of Fact 2:* Without loss of generality, let  $\theta_1, \theta_2 \in (-\pi, \pi]$ . This restriction does not lead to a loss of generality because  $\sin(\theta_1)$ ,  $\sin(\theta_2)$ , and  $N(\theta_1 - \theta_2)$  are periodic functions with period  $2\pi$ . Consider  $\theta_1 - \theta_2 > \pi$ . Thus,  $N(\theta_1 - \theta_2) = \theta_1 - \theta_2 - 2\pi$ . Since  $\sin(\cdot)$  function is periodic with period  $2\pi$ , we can rewrite (20) as

$$\frac{\sin(\theta_1) - \sin(\theta_2 + 2\pi)}{\theta_1 - (\theta_2 + 2\pi)}.$$

Therefore, (20) holds from Fact 1. The proof of the cases  $-\pi < \theta_1 - \theta_2 \le \pi$  and  $\theta_1 - \theta_2 \le -\pi$  are similar.

Proof of Lemma 4: On the contrary, assume that  $\theta_1^*$  and  $\theta_2^*$  be a solution different than the trivial solutions. Consider the case  $N(\theta_1^* - \theta_2^*) = 0$ . Equation (18) yields that  $\sin(\theta_1^*) = 0$  and  $\sin(\theta_2^*) = 0$ . Simultaneously satisfying these three equations contradicts with  $\theta_1^*$  and  $\theta_2^*$  are different than the trivial solutions. Consider the case  $N(\theta_1^* - \theta_2^*) \neq 0$ . Equation (18) yields that  $\sin(\theta_1^*)/N(\theta_1^* - \theta_2^*) = c_1$  and  $\sin(\theta_2^*)/N(\theta_1^* - \theta_2^*) = c_2$ . The subtraction of them gives  $(\sin(\theta_1^*) - \sin(\theta_2^*))/N(\theta_1^* - \theta_2^*) = c_1 - c_2$ . From Fact 2,  $-1 < c_1 - c_2 < 1$ . It contradicts with  $|c_1 - c_2| \geq 1$ .

## **REFERENCES**

- [1] H. Shakhatreh et al., "Unmanned aerial vehicles (UAVs): A survey on civil applications and key research challenges," *IEEE Access*, vol. 7, pp. 48572–48634, 2019.
- [2] A. A. Khuwaja, Y. Chen, N. Zhao, M.-S. Alouini, and P. Dobbins, "A survey of channel modeling for UAV communications," *IEEE Commun. Surv. Tut.*, vol. 20, no. 4, pp. 2804–2821, Fourthquarter 2018.
- [3] A. I. Alshbatat and L. Dong, "Adaptive MAC protocol for UAV communication networks using directional antennas," in *Proc. Int. Conf. Netw.*, Sens. Control, 2010, pp. 598–603.
- [4] H. N. Dai, K. W. Ng, M. Li, and M. Y. Wu, "An overview of using directional antennas in wireless networks," *Int. J. Commun. Syst.*, vol. 26, no. 4, pp. 413–448, 2013.
- [5] J. Zhang, H. Xu, L. Xiang, and J. Yang, "On the application of directional antennas in multi-tier unmanned aerial vehicle networks," *IEEE Access*, vol. 7, pp. 132095–132110, 2019.
- [6] L. Gupta, R. Jain, and G. Vaszkun, "Survey of important issues in UAV communication networks," *IEEE Commun. Surv. Tut.*, vol. 18, no. 2, pp. 1123–1152, Secondquarter 2016.
- [7] Y. Gu, M. Zhou, S. Fu, and Y. Wan, "Airborne WiFi networks through directional antennae: An experimental study," in *Proc. IEEE Wireless Commun. Netw. Conf.*, 2015, pp. 1314–1319.

- [8] J. Xie, F. Ai-Emrani, Y. Gu, Y. Wan, and S. Fu, "UAV-carried long-distance Wi-Fi communication infrastructure," in *Proc. AIAA Infotech, Aerosp.*, 2016, Art. no. 0747.
- [9] N. Malhotra, M. Krasniewski, C. Yang, S. Bagchi, and W. Chappell, "Location estimation in ad hoc networks with directional antennas," in *Proc. 25th IEEE Int. Conf. Distrib. Comput. Syst.*, 2005, pp. 633–642.
- [10] J. R. Jiang, C. M. Lin, F.-Y. Lin, and S. T. Huang, "ALRD: AoA localization with RSSI differences of directional antennas for wireless sensor networks," *Int. J. Distrib. Sensor Netw.*, vol. 9, no. 3, 2013, Art. no. 529489.
- [11] B. C. Min, J. Lewis, D. K. Schrader, E. T. Matson, and A. Smith, "Self-orientation of directional antennas, assisted by mobile robots, for receiving the best wireless signal strength," in *Proc. IEEE Sensors Appl. Symp. Proc.*, 2012, pp. 1–6.
- [12] J. Yan, Y. Wan, S. Fu, J. Xie, S. Li, and K. Lu, "Received signal strength indicator-based decentralised control for robust long-range aerial networking using directional antennas," *IET Control Theory Appl.*, vol. 11, no. 11, pp. 1838–1847, 2017.
- [13] J. Yan, H. Zhao, X. Luo, C. Chen, and X. Guan, "RSSI-based heading control for robust long-range aerial communication in UAV networks," *IEEE Internet Things J.*, vol. 6, no. 2, pp. 1675–1689, Apr. 2019.
- [14] J. Chen et al., "Long-range and broadband aerial communication using directional antennas (ACDA): Design and implementation," *IEEE Trans. Veh. Technol.*, vol. 66, no. 12, pp. 10793–10805, Dec. 2017.

- [15] S. Li et al., "Design and implementation of aerial communication using directional antennas: Learning control in unknown communication environments," *IET Control Theory Appl.*, vol. 13, no. 17, pp. 2906–2916, 2019
- [16] M. Liu, Y. Wan, S. Li, F. L. Lewis, and S. Fu, "Learning and uncertainty-exploited directional antenna control for robust long-distance and broadband aerial communication," *IEEE Trans. Veh. Technol.*, vol. 69, no. 1, pp. 593–606, Jan. 2020.
- [17] W. Zhu and D. Cheng, "Leader-following consensus of second-order agents with multiple time-varying delays," *Automatica*, vol. 46, no. 12, pp. 1994–1999, 2010.
- [18] R. G. Vaughan, "Pattern translation and rotation in uncorrelated source distributions for multiple beam antenna design," *IEEE Trans. Antennas Propag.*, vol. 46, no. 7, pp. 982–990, Jul. 1998.
- [19] H. K. Khalil, Nonlinear Systems. Upper Saddle River, NJ, USA: Prentice Hall, 2002.
- [20] J. Guckenheimer and P. Holmes, Nonlinear Oscillations, Dynamical Systems, and Bifurcations of Vector Fields, vol. 42. Berlin, Germany: Springer, 2013
- [21] L. Ljung, System Identification: Theory for the User, 2nd ed., Upper Saddle River, NJ, USA: Prentice Hall, 1987.